


REGULAR PAPER

Spray behaviour of hydro-treated ester fatty acids fuel made from used cooking oil at low injection pressures

Q. Azam¹, S.Z. Sulaiman², N. Abd Razak¹ and N.M. Mazlan¹

¹School of Aerospace Engineering, Engineering Campus, Universiti Sains Malaysia, Nibong Tebal, Pulau Pinang, Malaysia and

²Faculty of Chemical and Natural Resources Engineering, Universiti Malaysia Pahang, Kuantan, Pahang, Malaysia

Corresponding authors: N. M. Mazlan; Email: nmusfirah@usm.my

Received: 20 October 2022; **Revised:** 7 August 2023; **Accepted:** 10 August 2023

Keywords: Spray Characteristics; Used Cooking Oil; Biodiesel; Low Injection Pressures; Penetration Length; Particle Distribution

Abstract

The spray characteristics significantly affected the combustion performance. The injection pressure and fuel properties are factors that affect the spray cone angle, penetration, and droplet distribution. Although substantial research has been conducted on spray attributes, understanding the complex biofuel spray dynamics in real nozzles and injectors is crucial. This study examines hydro-processed esters and fatty acid (HEFA) spray characteristics of used cooking oil and palm oil biodiesel in a constant-volume chamber. The study was performed by varying the injection pressures ranging from 30 to 120psi for pure fuels and Jet A-1 blends. Experiments were conducted at standard sea-level atmospheric pressure and an ambient temperature of $\pm 297\text{K}$ using an airblast fuel injector. The initial fuel temperature was set at $\pm 302\text{K}$. Jet A-1 was used as the baseline fuel for the comparative analysis. Particle image velocimetry (PIV) was employed to visualise the microscopic and macroscopic characteristics of the fuel spray. The results revealed a progressive increase in the penetration length corresponding to an increase in the injection pressure. Lower pressures yielded non-uniform particle distributions across the spray area, whereas cone angle augmentation stabilised at elevated pressures. A blend of 60% Jet A-1 and 40% HEFA closely matched Jet A-1 characteristics, indicating alternative aviation fuel potential. These real-time insights into spray behaviour are critical for enhancing the fuel efficiency and mitigating the generation of particulate emissions resulting from spray combustion.

Nomenclature

ASI	start of injection
BD100	100% (pure) biodiesel
FAME	fatty acid methyl ester
H100	100% (pure) HEFA
HEFA	hydro-processed esters and fatty acids
J40H60	blend of 40% Jet A-1 with 60% HEFA
J50H50	blend of 50% Jet A-1 with 50% HEFA
PIV	particle image velocimetry
fps	frame per second
ms	millisecond
μm	micrometer
μs	microsecond

1.0 Introduction

Spray development and characteristics are essential for determining the combustion output of aircraft engines. The spray characteristics include cavitation, liquid breakup, atomisation and evaporation, all of

which are cross-related [1–3]. In a gas turbine combustor, liquid fuel is injected from the fuel injector, vaporised and atomized prior to combustion. The primary function of a fuel injector is to disperse fuel into small droplets [4]. The fuel is atomised to a significant number of droplets at a sufficient surface area to ensure high-quality ignition for proper air-fuel mixing to reduce engine emissions [5]. A smaller droplet size increases the atomisation rate, thereby improving the burning capacity of the fuel [6–8]. It is necessary for ignition to start at the flame front region near the injector head and to avoid combustion downstream of the chamber. A larger droplet size requires longer time to burn completely, thus producing high engine emissions. Therefore, a good droplet size distribution generated by the injection nozzle is necessary to achieve effective results.

The spray development can be fully understood through macroscopic and microscopic analyses. Microscopic analysis explains the droplet velocity and distribution, whereas macroscopic analysis provides information on spray penetration, spray angle and spray area [9, 10]. Marchione and Allouis [5] observed the mean diameter distributions, velocity profiles, cone angle variations and influence of spray fluctuation on the combustion stability of Jet A fuel at various air/fuel ratios. Combustion stability varies with the evaporation phenomenon and changes with different evaporation distribution functions. The interaction between temperature and pressure on evaporation was observed in a spray model tested on Jet A-1 fuel at pressures ranging from 1 to 15 bar [11]. Kwak et al. [12] developed spray and evaporation models to evaluate the spray penetration of multi-fuel mixtures in the quasi-dimensional multi-zone direct injection of an internal combustion engine for pressures ranging between 60–110MPa. Jing et al. [13] performed an experimental analysis of a jet fuel spray under different initial conditions, such as oxygen-rich inputs and ambient temperatures, to estimate the physical properties of the flame structure. Kannaiyan et al. [14] observed the relationship between fuel properties and injection pressure on spray characteristics. The results showed faster disintegration and dispersion of fuels with lower kinematic viscosities and surface tensions. Differences in the inertial forces and surface tension influence the mean axial velocity of the fuel, particularly at high injection pressures. Wang et al. [15] investigated the correlation between room temperature and low temperature on the droplet size and velocity of the fuel. Smaller spray areas and slower penetration were observed at low temperatures owing to the increase in viscosity [16]. However, the droplets are stable at low temperatures, resulting in spheroidal shapes. Gradual changes in the fuel injection velocity encourage droplet disintegration and immediate emanation from the nozzle [17, 18]. However, the expected results were less accurate at low pressure. The pressure was found to correlate with the liquid fuel primary breakdown period, which affected the momentum of the droplet particles during disintegration. Karimi [19] observed an equivalent fuel injection velocity with the jet velocity at the start of the injections. This finding demonstrates that the fuel can be modelled as a steady cylindrical body at an early stage of injection. This assumption was supported by Turner et al. [20], who found that the fluid core of the spray was maintained with a spray-line momentum that formed a steady and continuous injection from the nozzle exit.

The enhancement of the atomisation process depends mainly on the understanding of evaporation under a wide range of conditions. Most of the studies mentioned above observed a correlation between the ambient pressure, ambient temperature, injection velocity, fuel properties and fuel-air ratio on either the macroscopic or microscopic behaviour of Jet A-1. Although spray characteristics have been extensively studied, particularly in simple spray configurations, the spray dynamics of biofuels with complex geometries, such as real nozzles and fuel injectors, require further research to enhance the understanding of biofuel spray behaviour. As the aerospace industry has focused on potential sources of biofuels for aircraft engines, the details of macroscopic and microscopic spray characteristics of biofuels, such as hydro-treated ester fatty acids (HEFA) made from used cooking oil and biodiesel from palm oil at different injection pressures, are limited in the literature.

The scope of this study is to provide a detailed analysis of the microscopic and macroscopic behaviour of biofuel spray using a commercial jet engine atomiser. The study was performed experimentally, in which fuel samples were injected into a constant-volume chamber to represent the combustor chamber. The critical parameters related to the combustion characteristics, such as the fuel properties and injection pressures, were varied. In the present study, the absolute injection pressure was varied from 30 to

Table 1. Properties of the evaluation fuels

Properties	Method	J100	H100	J40H60	J50H50	BD
Density at @15°C (kg/m ³)	D1298	797.5	756.7	773.1	777	874.9
Surface tension (mN/m)		25.77	23.64	24.49	24.71	28.92
Viscosity @-20°C (mm ² /s)	D445	3.113	4.801	3.996	3.812	4.5
Flash point (°C)	D93	53	42	42	42	121
Freezing point (°C)		-50.3	-54.4	-59	59.6	-12.1
Specific energy (MJ/kg)	D3338	43.3	44.154	43.768	43.577	40.15
Boiling point (°C)	D86	260	277.6	276.5	276.3	-

120psi. To fully understand the influence of fuel properties and injection pressures on macroscopic and microscopic combustion characteristics, the ambient temperature and fuel temperature were kept constant. The ambient temperature was set to $\pm 297\text{K}$ and the fuel temperature was maintained at $\pm 302\text{K}$. It is hypothesised that the combination of fuel properties and injection pressures may provide variations in the flow features inside the chamber, thus providing advantages for the combustion characteristics. Therefore, the present study aims to fulfil the following research objectives:

1. To measure and compare microscopic and macroscopic parameters such as the droplet velocity, size and volume distribution frequency, spray penetration and spray cone angle of the selected fuels at the selected injection pressures.
2. The influence of the blended fuel ratio on the microscopic and macroscopic properties should be analysed in future studies.

This study elucidates the advantages and limitations of the aforementioned types of fuels for aerospace applications, particularly when sprayed using a conventional fuel injector used in aircraft engines.

2.0 Methodology

2.1 Materials

The two biofuels tested in the present study were hydrotreated ester fatty acids (HEFA) from used cooking oil and palm oil methyl ester (biodiesel). HEFA was obtained from SkyNRG, Netherlands, whereas biodiesel was obtained from FGV Biotechnologies Sdn. Bhd., Kuantan, Malaysia. HEFA is produced via hydrotreatment, cracking, isomerisation and distillation. Hydrotreatment eliminates oxygen from the oil sources and transforms them into hydrocarbons. The process of cracking and isomerisation produces a mixture of n-alkanes and iso-alkanes with excellent cold flow qualities, which are distilled and split into distinct products [21, 22]. Biodiesel is also known as a fatty acid methyl ester (FAME). Fuel is made by the trans-esterification of vegetable or animal fats with the addition of methanol. Biodiesel has characteristics similar to petroleum-derived diesel, including cetane number, energy content and viscosity [9]. In this study, biodiesel was tested as pure (BD100), whereas HEFA was tested as pure (H100) and blended with Jet A-1. The HEFA was blended at 60% (J40H60) and 50% (J50H50) with Jet A-1, respectively. Jet-A (J100) was used for comparison. The properties of the fuels and their blends are presented in Table 1.

2.2 Experimental set-up

The experiment was conducted at the Aerodynamics Research Laboratory at the School of Aerospace Engineering, Universiti Sains, Malaysia. Figure 1 shows a schematic of the experimental setup for the fuel spray.

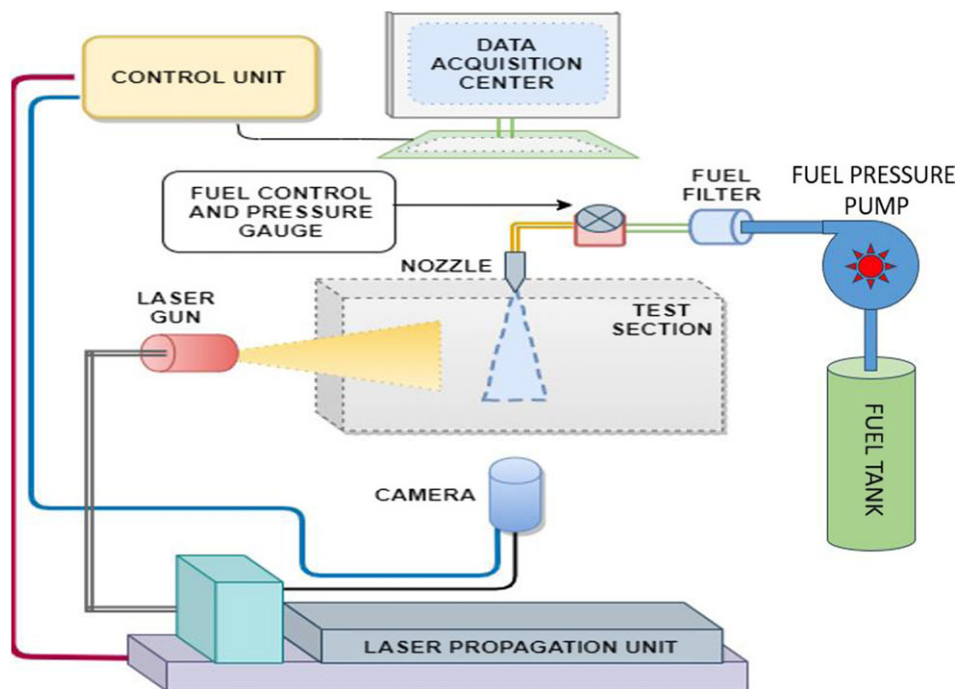


Figure 1. Schematic diagram of the experimental setup.

The setup consisted of a fuel pressure pump, fuel tank, fuel filter, fuel control, pressure gauge, nozzle, data acquisition unit and a high-speed camera. The fuels were stored in a fuel tank pressurised by compressed air supplied from the fuel pressure pump. A fuel filter was used to filter impurities in the fuel. A fuel injector was mounted vertically downward to ensure that the fuel spray was injected directly into the measurement test section. The fuel injector used in this study is a commercial fuel injector used in military aircraft engines. The test section was provided with a 40×30 cm rectangular viewing window that was sealed properly. Fuel control and pressure gauges were connected directly to the injector to control the injection pressure fluctuation during the test. The injection pressure was controlled using a pressure regulator located near the nozzle. The airblast atomiser nozzle has a hole with a diameter of $120 \pm 1 \mu\text{m}$. The atomiser range for the atomising droplet velocity was 180 m/s and the droplet size was $200 \mu\text{m}$ [23]. A constant-volume chamber with pressure and temperature of $\pm 297\text{K}$ was used. The fuel temperature was maintained at $\pm 302\text{K}$ using a centralised temperature regulator system attached to the experimental area. The injection pressure was varied from 30 to 120 psi. Each fuel sample was then sprayed for 20 s. The time taken for one captured image to another image was 0.1 seconds. The images were captured using a Dantec HiSense MKII C8484-52-05CP Hamamatsu C8484-05CP with a frame rate of 12.4 fps at full resolution. The time interval between images was 160 ms, with 20 frames producing 10 images captured in pairs in each acquisition procedure. In total, 200 images were captured for each sample. Before the experiment, the camera was calibrated using a trigger signal identical to that of the injector. PIV was calibrated by defining the calibration target. A series of calibration target images were captured using the same imaging setup and parameters. In addition, calibration was conducted by ensuring proper illumination and focusing to obtain high-quality images. In this study, the camera was programmed to capture standard focus pictures that covered almost every droplet particle. The focus point was set for all fuel sprays to capture the images. Capturing a series of images during the calibration process reduces the error and improves accuracy. A transitional form of the fuel spray was obtained by capturing spray images at various time steps. Spray images were interpreted using ImageJ and PIVlab

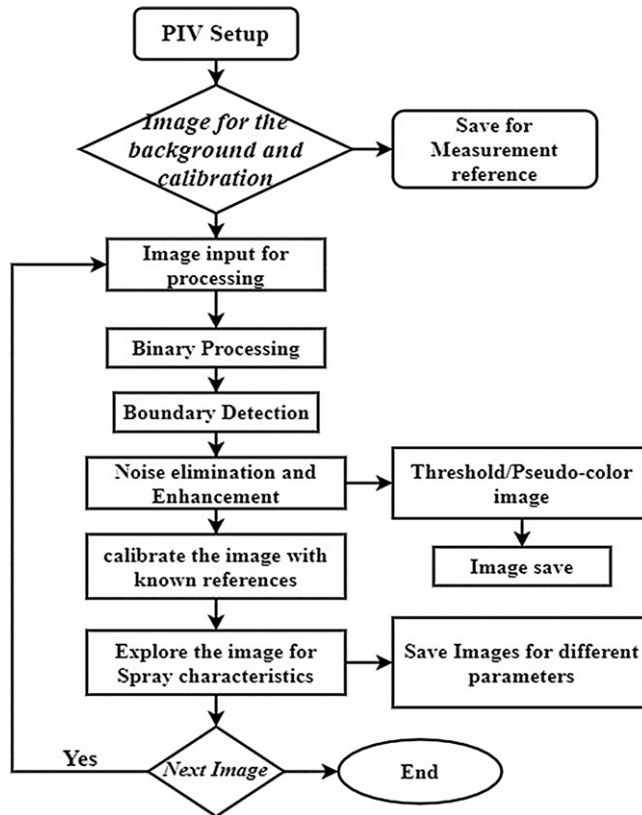


Figure 2. Flow chart showing the steps for image processing.

in MATLAB. Figure 2 shows a flowchart of the processing of the captured images. Initially, the background image is subtracted to distinguish the spray from the light reflected from the mirror window. The spray images were subjected to a threshold for visualisation and droplet detection was performed using Otsu's method [24]. Subsequently, edge detection was performed using the method suggested by Canny [25] to determine the area expansion of the spray.

3.0 Results and discussion

3.1 Macroscopic spray characteristics

3.1.1 The formation of spray

Figure 3 shows a sample of images of the spray formation of JetA-1 at an injection pressure of 30psi and 80% threshold analysis. The threshold analysis consists of 255 levels (i.e., from 0 to 255) within a pixel. The range of the specific percentage of the threshold reduced noise in the captured images. The 80% threshold analysis indicates the threshold analysis was performed at 204 level that converted the colour image to a black-and-white.

As soon as fuel was injected into the chamber, the fuel droplets began to disintegrate and form a mist at the end of the spray. Changes in droplet size were observed throughout the spray process. A reduction in droplet size can be found in three different regions after the start of injection (ASI). The first reduction in the droplet size was observed at $ASI = 120\mu\text{s}$, in which the diameter of the droplet reduces from 0.22 to $0.18\mu\text{m}$. The size of the droplet decreased further in the secondary breakup region ($ASI = 340\mu\text{s}$), where the size of the droplet reduces from 0.16 to $0.10\mu\text{m}$. Finally, the droplet was in the form of mist at $ASI = 620\mu\text{s}$.

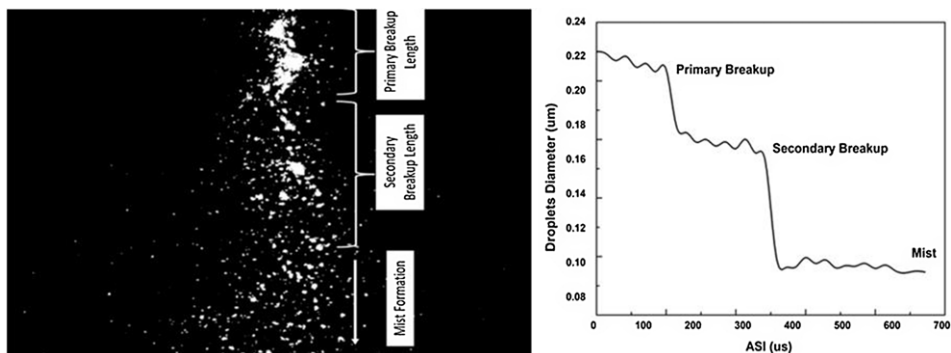


Figure 3. A typical captured spray image by PIV data acquisition system of Jet A-1 at 30psi.

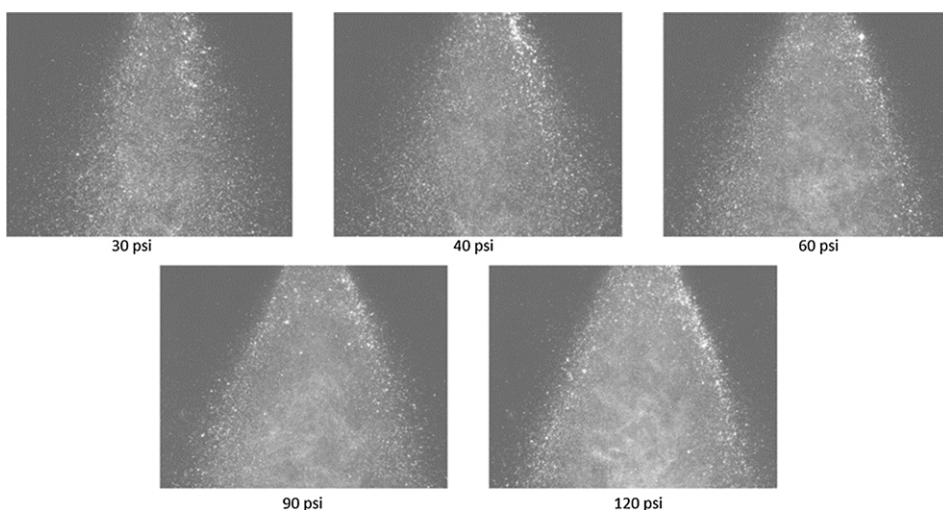


Figure 4. Spray image by PIV data acquisition system of Jet A-1 at the tested injection pressures.

The formation of Jet A-1 spray at various injection pressures is illustrated in Fig. 4. The spray droplet could be clearly seen at low injection pressures, whereas the formation of mist was more evident at higher injection pressures.

Figure 5 shows the spray formation comparison of each tested fuel measured at 120psi. This figure shows the dependency of spray formation on fuel properties, particularly the density and viscosity. BD100 had the lowest spray area and largest intact droplet size compared with the other tested fuels. The evaporation zone of BD100 was substantially longer than those of the other four samples. H100 injection produced smaller droplets and a broader spray zone. Similar patterns of spray development were observed for the J100 and blended samples.

The lengths of each breakup region are compared in Fig. 6. The presence of a breakup zone in the captured images was digitally improvised. The uncertainty in the interpretation of the optical measurements of these breakups was acknowledged in each instance. The majority of the quantitative information on the break-up zone has been collected from conductivity probe measurements made with fuel sprays and “break points” determined from penetration continuity. The length was obtained by measuring the distance between the two regions based on the diameter reduction discussed earlier. Generally, it was observed that the breakup lengths measured from the tip of the nozzle decreased with an increase in the injection pressure for all the tested fuels. At a particular injection pressure, BD100 had the highest

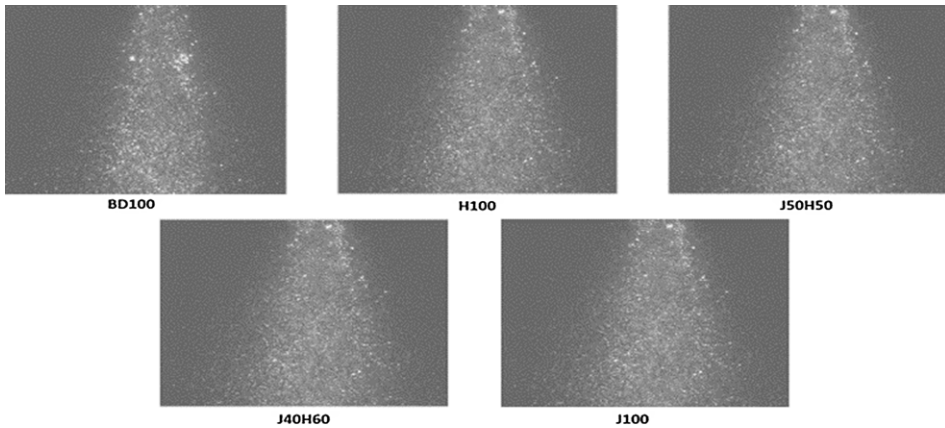


Figure 5. Five different tested fuel samples Spray image by PIV data acquisition system at 120psi.

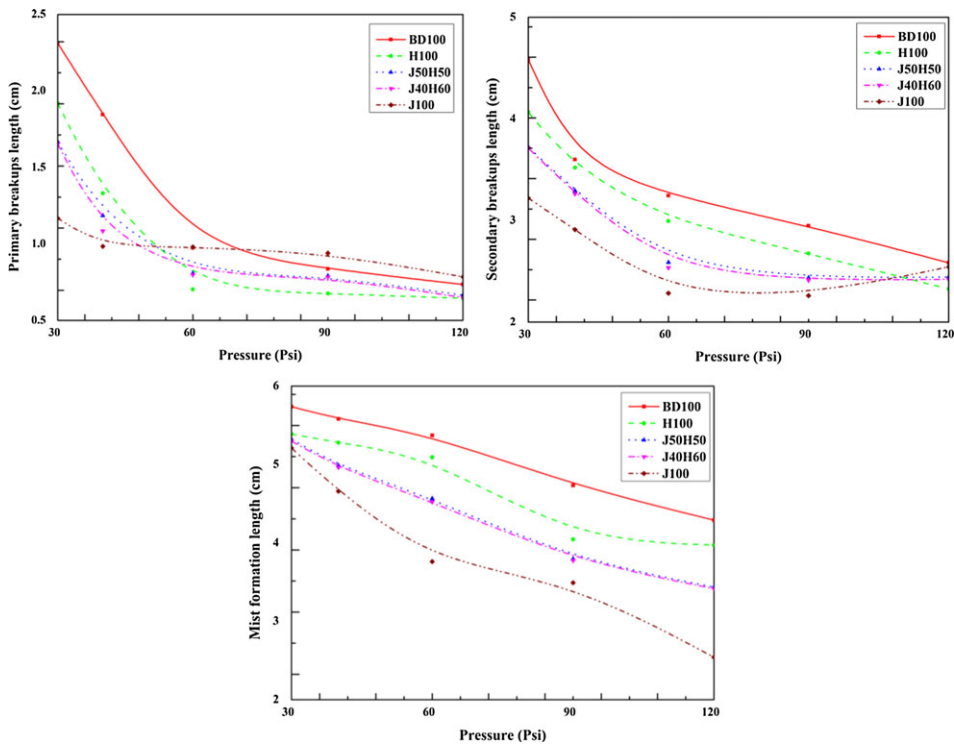


Figure 6. Breakup length at different injection pressure for primary breakup, secondary breakup and mist formation.

breakup length, whereas Jet A-1 had the shortest breakup length compared with the other tested fuels. This breakup is due to the unstable flow of sinuous disruption [26]. A higher rate of disruption breaks the liquid sheet at half-wavelength intervals into ligament droplets for mist formation [27].

3.1.2 Spray cone angle

The formation of the spray cone angle is significantly affected by the ambient density [28]. However, in this study, the ambient density was kept constant to investigate the influence of injection pressure on

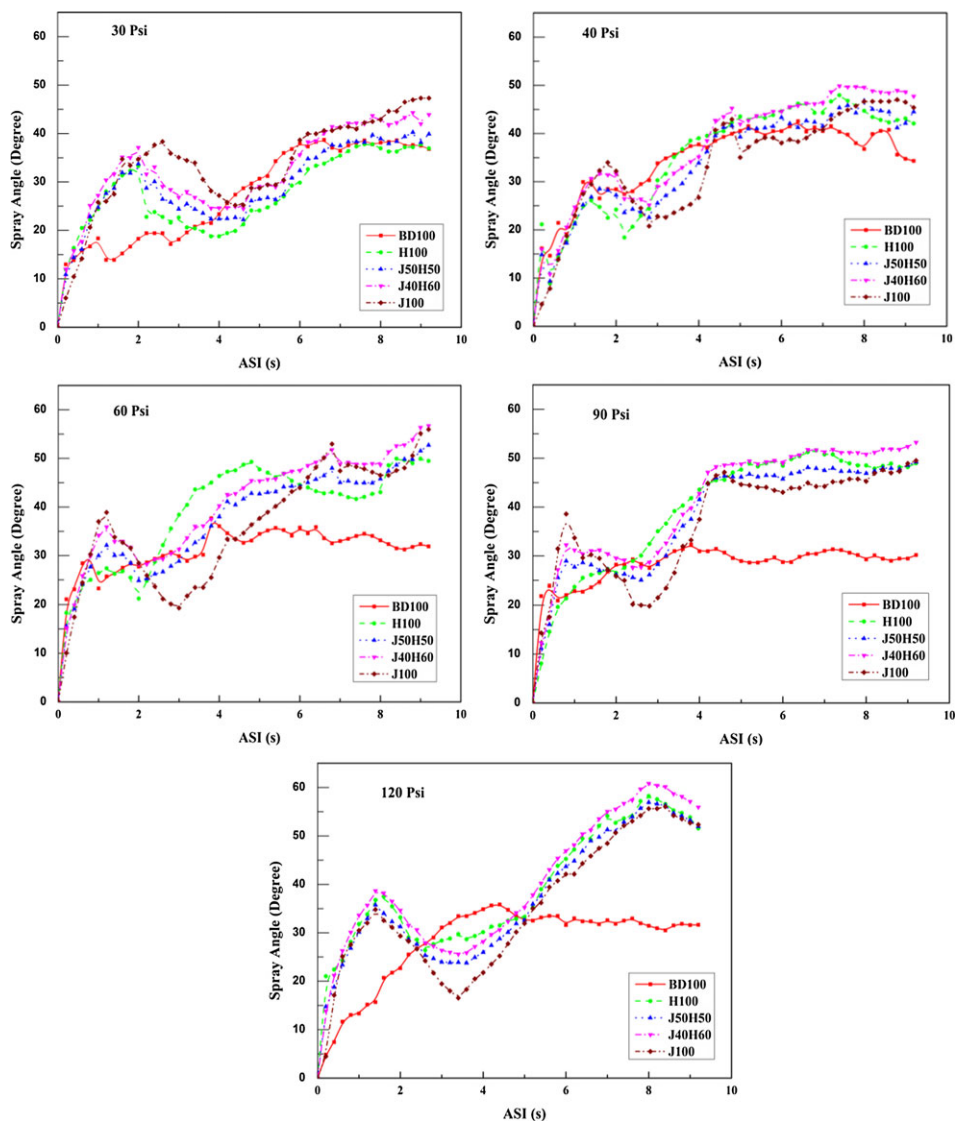


Figure 7. Influence of injection pressure with spray cone angle measured at the start of injection (ASI).

the spray cone angle. The cone angle was measured by detecting the spray boundaries from the spray images and the measured cone angle for every pair of captured images from the start of the injection until the end of a cycle of complete spray acquisition [29]. It is worth mentioning that the spray cone angle plays a crucial role in determining the fuel-air mixing, combustion efficiency and emission levels during gas turbine operation. The relationship between the spray cone angle and the aforementioned parameters was not investigated in this study. The spray cone angle measured in this study was only used to evaluate the formation of the cone angle for a wide range of fuel properties.

Figure 7 shows the variation in the spray cone angle recorded after the start of the injection (ASI) under various injection pressures. At each injection pressure, a fluctuation in the spray cone angle was observed during the early stages of the spray. However, the fluctuation became more stable after 1.2 milliseconds (ms). Once spray stability was achieved, a reduction in the spray cone angles was clearly observed as the injection pressure increased. Increasing the injection pressure was essential for evenly distributing the spray. At a low injection pressure, the spray area was dispersed more widely owing to

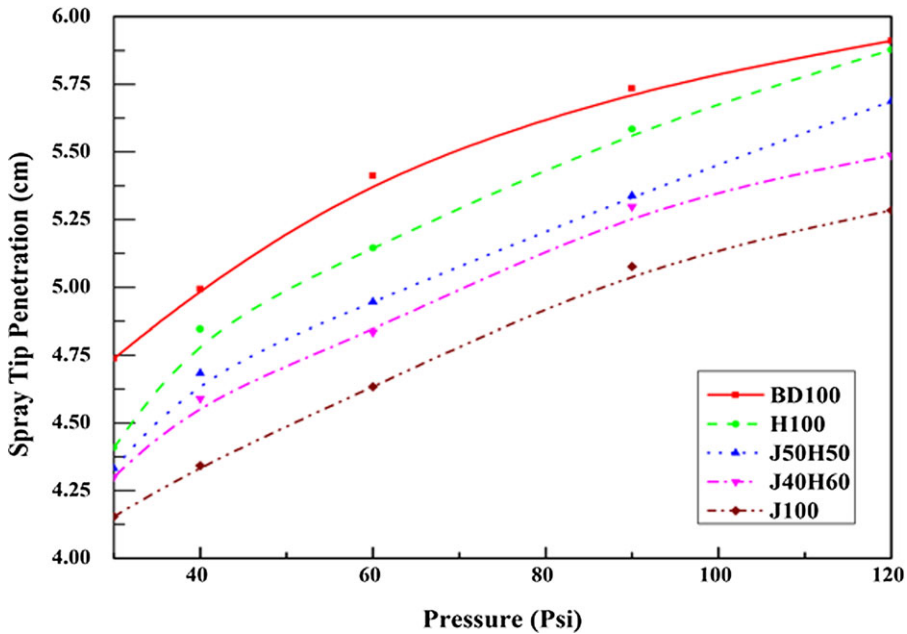


Figure 8. Spray tip penetration of the tested fuels at a various injection pressure.

the low velocity of the boundary particles than at higher injection pressures. The wide dispersion of the spray results in a larger spray cone angle. At a particular injection pressure, blending HEFA with Jet A-1 produced a lower spray cone angle than pure HEFA. The spray angle of the blend decreases as the percentage of HEFA in the blend decreases. The lowest spray cone angle was produced by the BD100.

The spray cone angles for each fuel are varied around 2–14% as injection pressure increased. The formation of the spray angle is more scattered at lower pressures. At higher pressures ($P = 120\text{psi}$), the spray angles of all fuels, except BD100, were closer to each other. The spray cone angle of BD100 decreased significantly as the pressure increased from 60 to 120psi. This reduction was due to the density and viscosity of BD100, which were higher than those of the other fuels tested. The fuel blends (J40H60 and J50H50) provided a maximum of 9% variation in the spray cone angle as the injection pressure increased from 30 to 60psi.

3.1.3 Spray tip penetration

Spray tip penetration is defined as the maximum distance of the spray after injection into stagnant or flowing air [30]. The spray penetration of jet fuel at various injection pressures is shown in Fig. 8. The spray penetration was measured at 0.2ms after the time start of injection. The correlation between fuel properties and penetration length can be observed by examining the total spray length at a particular injection pressure. The longest penetration was produced by BD100, whereas the shortest penetration was produced by Jet A-1. The longest penetration length of BD100 is associated with the higher density and surface tension of the fuel compared with other fuels. However, the surface tension did not affect the penetration length of H100. Although H100 had the lowest density and surface tension, the effect of viscosity on penetration length was highly significant. The same observation was made in Ref. (31), who observed a higher rate of particle disintegration and dispersion with a lower viscosity and density of fuel. In addition to fuel properties, turbulence, divergence, kinetic energy, particle collisions and aerodynamic forces contribute to the continual breakdown of fuel particles. Blending 60% of HEFA with 40% Jet A-1 provides closer penetration length with Jet A-1.

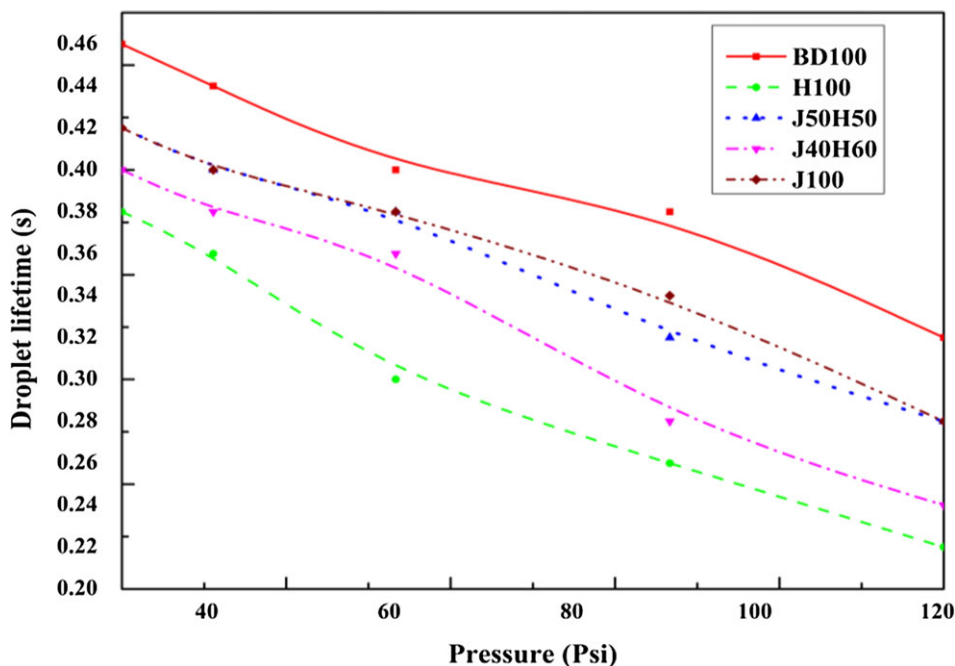


Figure 9. Evaporation time of the tested fuel at different injection pressure.

An increase in the injection pressure with spray length was clearly observed from 60 to 120psi. This trend is similar to those observed by Mohan et al. [32] and Kurachi et al. [33]. However, the increase in the penetration length with injection pressure was not identical at low pressures. As the pressure increased, the fuel with high density propagated longer than the low-density fuel. Despite the density, the viscosity of the fuel also contributed to spray tip penetration. The viscosities of J40H60 and J50H50 were lower than that of BD100. A lower viscosity tends to decrease the friction between the fuel and nozzle, thereby increasing the exit velocity. Similarly, J40H60 and J50H50 had lower densities than pure biodiesel, which enhanced the exit velocity. Droplets with lower viscosities are prone to deformation and breakup in later stages and produce significant momentum loss, restricting the propagation of the spray. The inertia of the fuel increases as the density increases, making it more resistant to the environment, thus allowing longer spray tip penetration. However, the effects of viscosity and density act accordingly in all zones during the spray development.

3.1.4 Droplet lifetime

Droplet lifetime is defined as the time required by a liquid particle to fully vaporise and evaporate. In a gas turbine engine, fuel is injected using an atomiser to produce fine droplets. The droplets evaporate and become vapour before mixing with air in the combustion chamber. Atomisation is required to increase the liquid area, thereby enhancing evaporation. The droplet lifetime defines the nature of the atomisation of the fuel; the fuel has a lower lifespan to evaporate proportionally to clean combustion. However, droplet lifetime plays a crucial role in evaporation and combustion. Figure 9 shows the evaporation times of the fuels at different injection pressures. The evaporation time was measured experimentally by recording the time taken by the particle after the start of injection until it diminished. The droplet lifetime decreased as the injection pressure increased from 30 to 120psi. Injecting the spray at 120psi resulted in the shortest evaporation time after the injection started. The longest injection time is observed at the lowest injection pressure. Injecting fuel at high pressure increases the droplet velocity. Because the fuel was injected into stagnant airflow, a large velocity difference was created between the

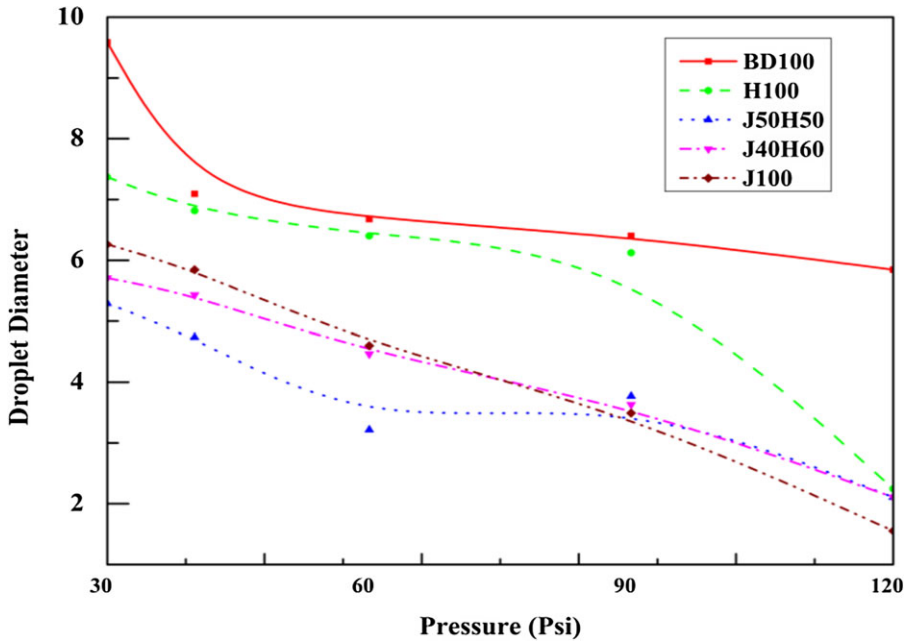


Figure 10. Droplet size (mm) distribution in axial direction at different injection pressure.

air and fuel spray. The large velocity difference enhanced the aerodynamic effects and developed turbulence, consequently promoting the disintegration of the fuel droplets. At a particular injection pressure, the BD100 droplet exhibited the longest lifetime, whereas the lowest droplet lifetime was observed for HEFA. A longer droplet lifetime was observed as the percentage of HEFA in the HEFA/Jet A-1 mixture decreased. The lifetime of the J50H50 droplet was closer to that of the Jet A-1 droplet at both lower and higher injection pressures. Under similar ambient conditions, fuels with lower viscosities and surface tensions exhibit rapid droplet disintegration and dispersion. Notably, in the present study, the droplet lifetime was measured under ambient conditions. The droplet lifetime of the fuel during the actual operation of a gas turbine engine is different. Droplet lifetime in a gas turbine engine is influenced by factors such as residence time, variation in droplet size, fuel properties, combustion conditions, turbulence and mixing, burner design and combustion system.

3.2 Microscopic spray characteristics

3.2.1 Mean droplet diameter (D10)

The mean droplet diameter (D10) is the average of all droplet diameters and provides information on the droplet size in the fuel spray sample. The D10 values of the tested fuels at various injection pressures are shown in Fig. 10 and were measured in millimeters. The mean diameter was calculated using the arithmetic mean diameter (D10) as shown in Equation (1): This equation was proposed by Ref. (31).

$$D_{10} = \frac{\sum_{i=1}^k D_i}{\sum_{i=1}^n N_i} \tag{1}$$

In Equation (1), N_i is the number of droplets with D_i diameter. In general, D10 is used to simplify the data analysis [34]. As shown in Fig. 10, the average droplet size decreased consistently as the injection pressure increased, except for J50H50, which exhibited a slight increase at higher injection pressures. As expected, the D10 of BD100 is the highest amongst the fuels, which explains the longest droplet

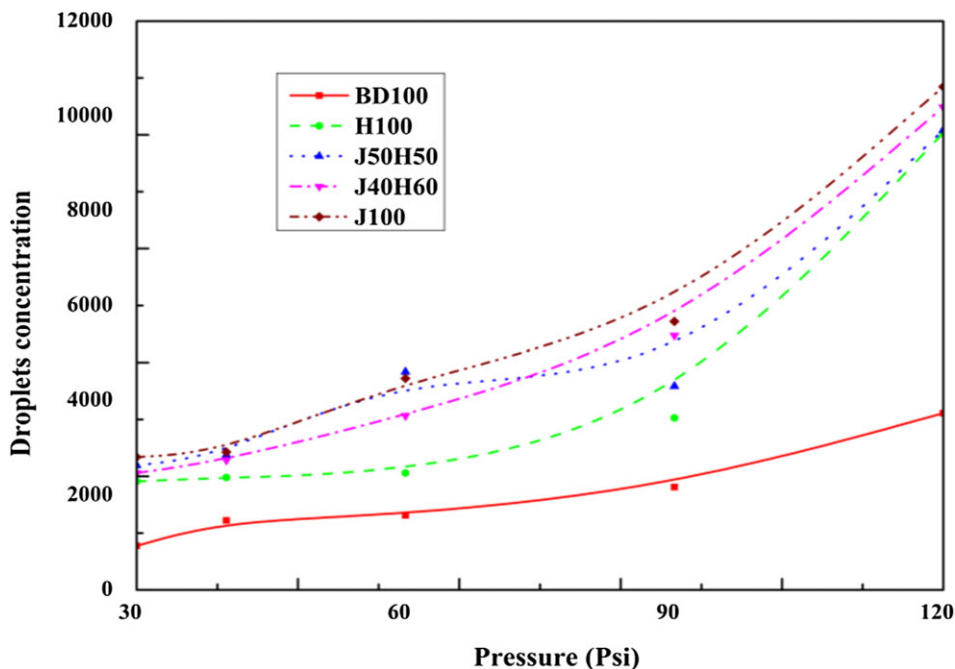


Figure 11. Number of droplets detected for each pressure.

lifetime of the fuel and shows a similar pattern to that of Fan et al. [29]. The difference in droplet size is associated with the kinematic viscosity and surface tension of the droplets throughout the spray [35].

3.2.2 Droplet concentration

Figure 11 illustrates the total number of average droplets counts in the spray region at various injection pressures by processing a captured image of a fully developed spray. Image processing in PIVlab software detected almost all droplets at an 80% threshold level. The number of droplets increased progressively as the injection pressure increased from 30 to 120psi. At lower injection pressures, the total number of droplets produced by HEFA, J50H50 and J40H60 was comparable to that of Jet A-1, which was approximately 930 droplets. As the injection pressure increased, Jet A-1 produced the highest number of droplets (approximately 10,614 droplets) compared with the other tested fuels. In contrast, the total number of droplets produced by BD100 was lower than those produced by the other fuels. The increase in the droplet number is also slower than that of other fuels, mainly owing to their viscous properties. According to this result, the spray droplet concentration is mainly determined by the continuous breakup of the spray droplets until mist formation and detection of all atomised droplets in the fuel spray region.

3.2.3 Droplet velocity profile

Figure 12 depicts the integral velocities of all the tested fuels and their profiles along the spray region at an injection pressure of 120psi. The integral velocity of the fuels was obtained directly from the PIV. PIV measures the particle velocity through a combination of the time interval and displacement of the particles between the two images. This result is consistent with those reported by Naber et al. [36] and Sieber [37]. Among the tested fuels, biodiesel produced the highest droplet velocity when the injection pressure was increased. Increases in the droplet velocity increase the Reynolds number of the droplet, causing the droplet to travel farther at higher injection pressures. The droplets travelled from the tip in

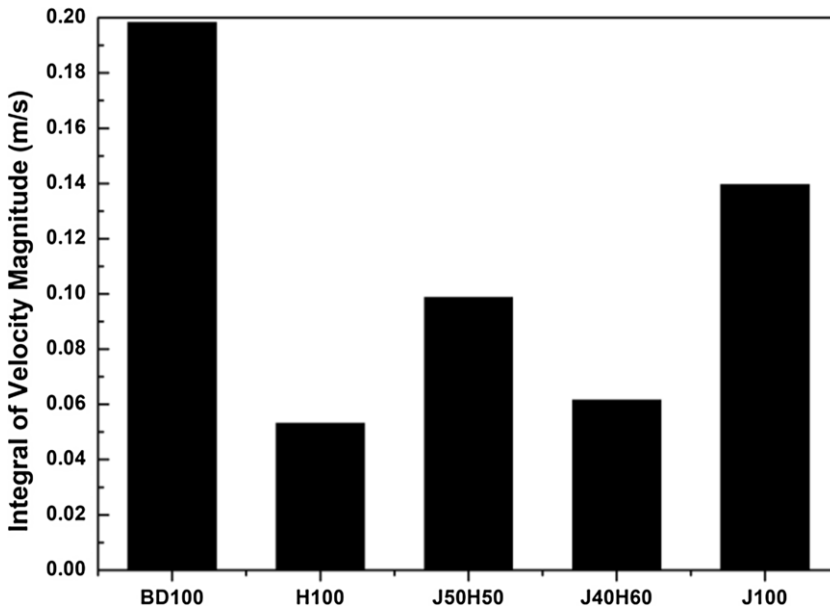


Figure 12. Integral of velocity magnitude from the tip of the nozzle as a function of axial direction at 120psi.

a downward direction and the individual velocity of the droplet decreased continuously. Consequently, the deformation of the fuel droplets will be smaller under the inertial force near the nozzle exit, in which the aerodynamic drag acting on the fuel droplets will be smaller. The velocity profile was calculated by comparative image sequence analysis using PIVlab software. Both HEFA and J40H60 showed similar results. Figure 12 shows the overall droplet velocity magnitude for the horizontal (u) and vertical (v) components along the spray length measured from the nozzle tip. The fluctuation in particle velocity is due to the formation of a vortex at a particular location. After a fuel droplet is injected into the combustion chamber, its motion is influenced by the turbulent vortex [38]. The turbulent vortex caused the droplet to move into a non-smooth curve instead of a straight line [39]. The development and quality of the spray structure are influenced by the formation and induction of vortices created by the velocity difference between the droplet and the ambient air. Soon after the formation, the wave shapes produced in the early injection stage disappeared, and the spray patterns began to recover uniform shapes. However, increasing the pressure minimised the fluctuation in the spray tip velocity.

4.0 Conclusion

This study presents the macroscopic and microscopic spray characteristics of biodiesel, HEFA and its blends with Jet A-1 at various injection pressures, using a commercial aircraft fuel injector nozzle for real-time analysis under normal ambient conditions. The vertical spraying setup was attached to a constant volume test section. The study observed insignificant spray cone angle differences in the axial direction of Jet A-1, HEFA and their blend samples. The penetration length of the droplet gradually increased with increasing pressure; however, the area of the spray increased more extensively at moderate pressures. BD100 reached its maximum length, whereas J100 exhibited its minimum penetration length. Blended fuels provided remarkable penetration results, with a 3.6% difference each. The spray particle distribution was nonuniform throughout the spray area, particularly at low pressures. Increasing the injection pressure increases the particle velocity. The developed mist and spray film boundaries were visualised around the secondary breakup region. The cone angle increased with increasing pressure and remained stable at high pressures. The effects of the viscosity, density and surface tension on the spray

characteristics were observed. BD100 provided the longest spray penetration and droplet lifetime owing to its poor fuel properties compared with the other tested fuels. As far as the blended fuel is concerned, blending 60% with 40% Jet A-1 (J40H60) is observed to have comparative spray characteristics and features to those Jet A-1 fuel; thus has a potential as future optional fuel for the aviation industry.

The present study is an initial step towards the establishment of a simulation in FLUENT to measure the spray characteristics of real conditions of gas turbine operation.

Acknowledgment. The authors would like to express their gratitude to the Malaysian Government's Fundamental Research Grant Scheme (FRGS/1/2019/TK07/USM/03/5) and USM Fellowship Scheme for providing funding for this study. Additionally, the authors extend their thanks to Mr. Mohd Najib Mohd Hussain, senior assistant engineer of the School of Aerospace Engineering, for his valuable assistance during the experiments.

Competing interests. The author(s) declare none.

References

- [1] Lahane, S., Deshmukh, P.W. and Nandgaonkar, M.R. Mathematical modeling of injection and spray characteristics of a diesel engine: a review, in *Energy, Environment, and Sustainability*, 2022, pp 29–55. https://doi.org/10.1007/978-981-16-8618-4_3
- [2] Heidari-Koochi, M., Karathanassis, I., Koukouvinis, P., Hwang, J., Pickett, L., Spivey, D. and Gavaises, M. Flow visualisation in real-size optical injectors of conventional, additised, and renewable gasoline blends, *Energy Convers Manag.*, 2022, **252**. <https://doi.org/10.1016/j.enconman.2021.115109>
- [3] Cho, J., Lee, D., Kang, T.G. and Moon, H. Study on spray characteristics of simulant gel in pressure swirl injector, *Int. J. Aeronaut. Space Sci.*, 2022. <https://doi.org/10.1007/s42405-022-00504-0>
- [4] Yoo, Y., Lee, H., Choi, H., Jeong, B. and Han, J. Influence of fuel boiling point on discharge characteristics of superheated hydrocarbon liquid jets, *Int. J. Aeronaut. Space Sci.*, 2020, **21**, pp 186–200. <https://doi.org/10.1007/S42405-019-00214-0>
- [5] Marchione, T., Allouis, C., Amoresano, A. and Beretta, F. Experimental investigation of a pressure swirl atomizer spray, *J. Propul. Power*, 2007, **23**, pp 1096–1101. <https://doi.org/10.2514/1.28513>
- [6] Laryea, G.N. and No, S.Y. Spray angle and breakup length of charge-injected electrostatic pressure-swirl nozzle, *J. Electrostat.*, 2004, **60**, pp 37–47. <https://doi.org/10.1016/j.elstat.2003.11.001>
- [7] Xia, J., Huang, Z., Zhang, L., Zhang, Q., Zheng, L., Liu, R., Ju, D. and Lu, X. Experimental comparisons on injection and atomization characteristics of diesel and its six-component surrogate under different critical conditions of marine engine, *Energy Convers. Manag.*, 2020, **205**. <https://doi.org/10.1016/j.enconman.2019.112397>
- [8] Azam, Q., Alhaj, A.M., Janvekar, A.A. and Mazlan, N.M. A review on alternative fuel spray characteristics, Proceedings of International Conference of Aerospace and Mechanical Engineering 2019. Lecture Notes in Mechanical Engineering, Springer, 2020, Singapore. https://doi.org/10.1007/978-981-15-4756-0_1
- [9] Taşkıran, Ö.O. and Ergeneman, M. Experimental study on diesel spray characteristics and autoignition process, *J. Combust.*, 2011, **2011**, p 12. <https://doi.org/10.1155/2011/528126>
- [10] Lee, M., Lee, G., Kim, C., Seo, J. and Kim, K. Macroscopic and microscopic spray characteristics of diesel and gasoline in a constant volume chamber, *Energies (Basel)*, 2018, **11**. <https://doi.org/10.3390/en11082056>
- [11] Harstad, K. and Bellan, J. Modeling evaporation of Jet A, JP-7, and RP-1 drops at 1 to 15 bars, *Combust. Flame*, 2004, **137**, pp 163–177. <https://doi.org/10.1016/j.combustflame.2004.01.012>
- [12] Kwak, K.H., Jung, D. and Borgnakke, C. Enhanced spray and evaporation model with multi-fuel mixtures for direct injection internal combustion engines, *Int. J. Eng. Res.*, 2014, **15**, (4), pp 488–503. doi: 10.1177/1468087413495203
- [13] Zhang, J. and Fang, T. Spray combustion of biodiesel and diesel in a constant volume combustion chamber (No. 2011-01-1380). SAE Technical Paper, 2011.
- [14] Kumar, M., Karmakar, S., Kumar, S. and Basu, S. Experimental investigation on spray characteristics of Jet A-1 and alternative aviation fuels, *Int. J. Spray Combust. Dyn.*, 2021, **13**, pp 54–71. <https://doi.org/10.1177/17568277211010140>
- [15] Wang, Z., Jiang, C., Xu, H. and Wyszynski, M.L. Macroscopic and microscopic characterization of diesel spray under room temperature and low temperature with split injection, *Fuel Process. Technol.*, 2016, **142**, pp 71–85. <https://doi.org/10.1016/j.fuproc.2015.10.007>
- [16] Algayyim, S.J.M. and Wandel, A.P. Macroscopic and microscopic characteristics of biofuel spray (biodiesel and alcohols) in CI engines: a review, *Fuel*, 2021, **292**. <https://doi.org/10.1016/j.fuel.2021.120303>
- [17] Dafsari, R.A., Vashahi, F. and Lee, J. Effect of swirl chamber length on the atomization characteristics of a pressure-swirl nozzle, *Atomization Sprays*, 2017, **27**, pp 859–874. <https://doi.org/10.1615/AtomizSpr.2017024777>
- [18] Gorokhovski, M.A. and Saveliev, V.L. Analyses of Kolmogorov's model of breakup and its application into Lagrangian computation of liquid sprays under air-blast atomization, *Phys. Fluids*, 2003, **15**, pp 184–192. <https://doi.org/10.1063/1.1527914>
- [19] Karimi, K. Characterisation of Multiple-Injection Diesel Sprays at Elevated Pressures and Temperatures, Doctoral Dissertation, University of Brighton, 2007.
- [20] Turner, M.R., Sazhin, S.S., Healey, J.J., Crua, C. and Martynov, S.B. A breakup model for transient Diesel fuel sprays, *Fuel*, 2012, **97**, pp 288–305. <https://doi.org/10.1016/j.fuel.2012.01.076>
- [21] Gawron, B. and Białecki, T. Impact of a Jet A-1/HEFA blend on the performance and emission characteristics of a miniature turbojet engine, *Int. J. Environ. Sci. Technol.*, 2018, **15**, pp 1501–1508. <https://doi.org/10.1007/S13762-017-1528-3>

- [22] Zschocke, A., Scheuermann, S. and Ortner, J. High biofuel blends in aviation (HBBA). Interim Report, ENER C, 2, 2017, pp 420–421.
- [23] Lorenzetto, G.E. and Lefebvre, A.H. Measurements of drop size on a plain-jet airblast atomizer, 2012, **15**, pp 1006–1010. <https://doi.org/10.2514/3.60742>
- [24] Bester, N. and Yates, A. Assessment of the operational performance of fischer-tropsch synthetic-paraffinic kerosene in a T63 gas turbine compared to conventional jet A-1 fuel, Proceedings of the ASME Turbo Expo 2009: Power for Land, Sea, and Air. Volume 2: Combustion, Fuels and Emissions, Orlando, Florida, USA. June 8–12, 2009, ASME, 2009, pp 1063–1077. <https://doi.org/10.1115/GT2009-60333>
- [25] Canny, J. A computational approach to edge detection, *IEEE Trans. Pattern Anal. Mach. Intell.*, 1986, **PAMI-8**, pp 679–698. <https://doi.org/10.1109/TPAMI.1986.4767851>
- [26] Chen, J., Li, G. and Zhang, T. Analysis of characteristics of swirling spray of the ammonium dinitramide (ADN)-based green monopropellant, *Int. J. Aeronaut. Space Sci.*, 2018, **19**, pp 926–931. <https://doi.org/10.1007/S42405-018-0085-4>
- [27] Sivakumar, D., Vankeswaram, S.K., Sakthikumar, R., Raghunandan, B.N., Hu, J.T.C. and Sinha, A.K. An experimental study on jatropa-derived alternative aviation fuel sprays from simplex swirl atomizer, *Fuel*, 2016, **179**, pp 36–44. <https://doi.org/10.1016/j.fuel.2016.03.050>
- [28] Yu, S., Yin, B., Deng, W., Jia, H., Ye, Z., Xu, B. and Xu, H. Experimental study on the spray characteristics discharging from elliptical diesel nozzle at typical diesel engine conditions, *Fuel*, 2018, **221**, pp 28–34. <https://doi.org/10.1016/j.fuel.2018.02.090>
- [29] Fan, Y., Hashimoto, N., Nishida, H. and Ozawa, Y. Spray characterization of an air-assist pressure-swirl atomizer injecting high-viscosity Jatropa oils, *Fuel*, 2014, **121**, 271–283. <https://doi.org/10.1016/J.FUEL.2013.12.036>
- [30] Lim, J., Razak, N.A. and Mazlan, N.M. An evaluation of alternative fuels' spray penetration at various spray cone angles and injection pressures using a simple evaporation model, *Biofuels*, 2022, **13**, pp 321–331. <https://doi.org/10.1080/17597269.2019.1693180>
- [31] Kumar, M., Karmakar, S., Kumar, S. and Basu, S. Experimental investigation on spray characteristics of Jet A-1 and alternative aviation fuels, *Int. J. Spray Combust. Dyn.*, 2021, **13**, pp 54–71. <https://doi.org/10.1177/17568277211010140>
- [32] Mohan, B., Yang, W., Tay, K.L. and Yu, W. Macroscopic spray characterization under high ambient density conditions, *Exp. Therm. Fluid Sci.*, 2014, **59**, pp 109–117. <https://doi.org/10.1016/j.expthermflusci.2014.08.003>
- [33] Kurachi, K., Serizawa, T., Wada, K., Kato, S. and Ito, H. Investigation on measurement of diesel spray breakup length by using doppler signals, *SAE Trans.*, 2001, **110**, pp 449–455. <http://www.jstor.org/stable/44724320>
- [34] Mayhew, E. and Wood, E. BM-A and, 2021 undefined High-speed phase contrast imaging of spray breakup of jet fuels under combusting conditions. dl.begellhouse.com
- [35] Lee, K. and Reitz, R.D. Investigation of spray characteristics from a low-pressure common rail injector for use in a homogeneous charge compression ignition engine, *Meas. Sci. Technol.*, 2004, **15**, pp 509–519. <https://doi.org/10.1088/0957-0233/15/3/003>
- [36] Naber, J.D. and Siebers, D.L. Effects of Gas Density and Vaporization on Penetration and Dispersion of Diesel Sprays, SAE Technical Paper 960034, 1996.
- [37] Siebers, D.L. Liquid-Phase Fuel Penetration in Diesel Sprays, SAE Technical Paper 980809, 1998.
- [38] Du, S., Al-Rashed, A., Barzegar Gerdroodbary, M., Moradi, R., Shahsavari, A. and Talebizadehsardari, P. Effect of fuel jet arrangement on the mixing rate inside trapezoidal cavity flame holder at supersonic flow, *Int. J. Hydrogen Energy*, 2019, **44**, pp 22231–22239. <https://doi.org/10.1016/j.ijhydene.2019.06.020>
- [39] Yin, L., E, J., Ding, J. and Li, Y. An experimental study on the spray characteristics of splash platelet injector, *Acta Astronaut.*, 2021, **181**, pp 377–383. <https://doi.org/10.1016/j.actaastro.2021.01.046>